Fuzzy-Enhanced Dual Phase Shift PWM Strategy for Bidirectional Wireless Charging in EV Applications

A.CHAKRADHAR , Assistant Professor of Department of ELECTRICAL & ELECTRONICS ENGINEERING, Sanketika Institute A Technology and Management (SITAM)
Visakhapatnam, Andhra Pradesh, India.
Email id: chakradhar.eee@svpec.edu.in

A.NIKHITHA , Student of B-TECH, Sanketika Institute A Technology and Management (SITAM) affiliated to Jawaharlal Nehru Technological University, Gurajada Vizianagaram (JNTUGV)
Visakhapatnam, Andhra Pradesh, India. Email id: nikithaarangi@gmail.com

Y.GANESH VENKATA VARDHAN , Student of B-TECH, Sanketika Institute A Technology and Management (SITAM) affiliated to Jawaharlal Nehru Technological University, Gurajada Vizianagaram (JNTUGV)
Visakhapatnam, Andhra Pradesh, India. Email id: ganeshyelleti58@gmail.com

SANAPATHI SYAM KUMAR , Student of B-TECH, Sanketika Institute A Technology and Management (SITAM) affiliated to Jawaharlal Nehru Technological University, Gurajada Vizianagaram (JNTUGV)
Visakhapatnam, Andhra Pradesh, India. Email id: shyamkumarsanapathi@gmail.com

M V VISWA SHANMUKHA GANESH, Student of B-TECH, Sanketika Institute A Technology and Management (SITAM) affiliated to Jawaharlal Nehru Technological University, Gurajada Vizianagaram (JNTUGV)
Visakhapatnam, Andhra Pradesh, India. Email id: shanmukhganesh123@gmail.com

ABSTRACT

To support seamless Grid-to-Vehicle (G2V) and Vehicle-to-Grid (V2G) operations, Bidirectional Wireless Power Transfer (BWPT) eliminates manual intervention but still faces challenges such as power factor control, efficiency, and limited transfer rates. This research proposes a Dual Phase Shift Pulse Width Modulation (DPS-PWM) technique aimed at improving Power Factor Correction (PFC) in BWPT systems. Additionally, a Fuzzy Logic Controller (FLC) is integrated to enhance the dynamic response and optimize switching decisions in real-time based on input variations and system behavior.

The proposed intelligent control strategy is evaluated through both simulation and experimental setups operating at 85 kHz and 3.7 kW. MATLAB/Simulink is used to model and simulate the BWPT system, allowing in-depth performance analysis under diverse operating conditions. Results indicate a power transfer efficiency of 94.4% in simulation and 90.1% in experiment, with notable improvements in Total Harmonic Distortion (THD) and overall

system robustness. The integration of fuzzy logic demonstrates significant potential for adaptive and efficient control in next-generation BWPT systems for electric vehicles.

I. OVERVIEW

The growing concern over environmental sustainability and the depletion of fossil fuels has significantly influenced the automotive industry, accelerating research and development in the electric vehicle (EV) sector [1]. One of the most critical challenges hindering the widespread adoption of EVs is the efficiency and convenience of the charging process. Key concerns include long recharge times, safety risks, and the need for human intervention.

Wireless Power Transfer (WPT) technology offers a promising solution by enabling contactless energy transfer from a power source to a load. WPT enhances user convenience and safety compared to conventional wired charging methods [2]. By eliminating the need for charging cables, this technology not only simplifies the charging process but also reduces risks associated with physical connections. Moreover, the ability to charge without human involvement supports lighter and more compact battery designs, shorter charging intervals, and the flexibility to charge devices anywhere a compatible outlet is available [3].

Beyond EVs, WPT is also being applied in various high-power and specialized applications, such as railway traction systems, underwater vehicles, and the wireless powering of medical implants [4], [5]. These applications underscore the broader potential of WPT in addressing the limitations of battery-powered systems, such as restricted battery life and high upfront costs. The attributes of WPT—including high reliability, user convenience, operational safety, and resilience to environmental conditions—contribute to its growing adoption [6].

In particular, **Bidirectional Wireless Power Transfer (BWPT)** plays a vital role in enabling emerging technologies like Vehicle-to-Home (V2H), Vehicle-to-Vehicle (V2V), and Vehicle-to-Grid (V2G), all of which depend on bidirectional energy flow. Modern BWPT systems incorporate fully controlled switching devices such as SiC MOSFETs and IGBTs to achieve high-frequency operation across both primary and secondary bridges. Figure 1 illustrates a typical block diagram depicting the integration of photovoltaic (PV) systems, wirelessly connected EVs, a DC bus, and the power grid in V2G and G2V scenarios. By participating in active and reactive power management, EVs contribute to improved power quality and enhanced grid stability [7].

Furthermore, seamless integration of EVs, the power grid, and Renewable Energy Systems (RES) promotes higher RES penetration and usage efficiency [8]. However, achieving this integration requires robust and continuous bidirectional communication, particularly during EV charging and discharging operations.

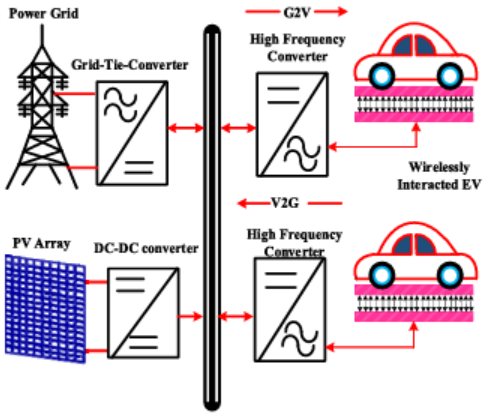

FIGURE 1. Illustration of wirelessly interconnected EVs in the V2G and G2V service.

In grid-connected systems, maintaining the power factor and Total Harmonic Distortion (THD) within acceptable limits is essential. Power electronic converters used in wireless charging systems play a critical role in preserving power quality. However, various uncertainties—such as coil misalignment, parameter detuning, fluctuations in coil distance, and load variation—can cause the Wireless Power Transfer (WPT) system to deviate from its optimal performance [9]. These deviations can lead to reduced power transfer efficiency, increased power losses, soft switching challenges, and greater stress on components. Among these, maintaining a high power factor is particularly vital to ensure smooth integration of Bidirectional Wireless Power Transfer (BWPT) systems with the power grid.

To achieve this, the wireless charger design must prioritize power factor correction. Employing appropriate resonant compensation networks on both the primary and secondary sides of the system can significantly enhance power transfer efficiency [10]. Various compensation topologies have been proposed, particularly for unidirectional WPT systems, to manage voltage and current variations. Typically, compensation tanks are added to the AC link of both bridges to improve transmission efficiency and system capacity.

Among the available topologies, the LCC-compensated BWPT system has gained considerable attention due to its symmetrical structure, improved tolerance to load variations, and reduced sensitivity to changes in the coupling coefficient [11]. On the primary side, LCC compensation effectively addresses issues associated with series (S) compensation by converting the voltage source into a current source using an inverter. This configuration ensures a steady current in the primary coil, thereby preventing overcurrent conditions and improving performance [12]. Even under light load conditions, the LCC resonance compensation circuit contributes to higher output voltage stability.

In conventional BWPT systems, the direction and magnitude of active and reactive power flows are controlled by the relative phase angle and amplitude of the voltages generated by the full-bridge inverters on both primary and secondary sides [13]. Although synchronization of these switching signals can be achieved via wireless communication interfaces, this approach increases system complexity and reduces robustness. An alternative method eliminates the need for wireless communication by leveraging the active and reactive power control capabilities of the secondary-side inverter for synchronization [14], [15]. In this approach, the flow of real and reactive power continues to depend on the characteristics of passive

components, the phase angle, and the voltage amplitudes on both sides of the full-bridge inverters.

Recent advancements in WPT circuit design have shifted focus from single-sided to double-sided compensation strategies. These approaches offer greater design flexibility and are better suited to meet the evolving performance demands of modern WPT systems [15].

Efficient power regulation—from an unregulated AC output to a regulated DC output—is essential in high-frequency Wireless Power Transfer (WPT) systems, especially for Electric Vehicle (EV) battery charging. To enhance power density, integrated Power Factor Correction (PFC) circuits have been proposed as an alternative to conventional front-end PFC methods, which typically rely on bulky passive components [16]. Despite concerns about battery lifespan, integrating EVs with renewable and grid resources is expected to offer financial benefits to both grid operators and EV owners. To reduce system costs, PFC has also been implemented on the secondary side of WPT systems [17]. However, this approach introduces additional circuit complexity [2].

The LCCL compensation topology plays a key role in maintaining a stable output voltage at the secondary side, which is vital for consistent control of the connected DC–DC converter responsible for battery charging [3]. To manage this, a hybrid LCC-Series (LCC-S) compensation technique is utilized, allowing for flexible output voltage adjustment in the WPT system [18]. When combined with phase shift modulation and a switch-controlled capacitor, the LCC-S technique enables wide-range output voltage regulation [4], [18], [19]. A 500-W prototype operating with an input of 400 V and a variable output of 100–250 V demonstrated a maximum efficiency of 94.1%, while achieving Zero Voltage Switching (ZVS) across the voltage range [19].

Furthermore, a dual-side LCC-LCC compensated WPT converter has been analyzed for generating load-independent Constant Voltage (CV) and Constant Current (CC) outputs at zero-phase angular frequencies. This dual-side compensation strategy provides a systematic design framework and achieves a lighter and more compact system compared to traditional WPT topologies. By incorporating advanced Analog Phase Control (APC) and Digital Phase Control (DPC) methods, the converter simplifies its control system while supporting both CV and CC operating modes [6], [7]. A combination of simulation and experimental data confirms the viability of this approach.

To regulate power transfer without large passive components, the role of secondary active converters has gained attention. Conventional WPT systems typically use front-end PFC stages that contribute to increased volume, power loss, and reduced reliability. Due to the absence of intermediate energy storage on the primary side, synchronization between the primary and secondary bridges often relies on complex algorithms [7].

To address these challenges, a novel **fuzzy logic-based phase shift control strategy** was introduced for Full-Bridge Active Rectifiers (F-BARs) in Bidirectional Wireless Power Transfer (BWPT) systems. This approach removes the need for direct communication between the transmitter and receiver by dynamically adjusting the output using fuzzy rules based on voltage and current deviations. Simulation and theoretical analysis confirm that this fuzzy logic control mechanism achieves efficient output regulation. The system reached a peak efficiency

of 94.4% at an input voltage of 325 V DC with output power ranging from 0 to 3.7 kW. Experimental results further validate the converter's performance and the effectiveness of the proposed fuzzy-based control strategy.

The key contributions of this work include:

- Implementation of **dual-side fuzzy logic phase shift control**, enhancing power factor and enabling robust bidirectional power regulation.
- Detailed performance evaluation of the proposed BWPT strategy, including frequency bifurcation, THD, and power loss analysis.
- Experimental validation and modeling of the dual-side fuzzy-controlled BWPT system.

Section II outlines the modes of BWPT operation, while Section III discusses alternative control strategies with an emphasis on fuzzy logic-based phase shift modulation. Section IV details the bidirectional power control mechanisms between Grid-to-Vehicle (G2V) and Vehicle-to-Grid (V2G). Section V describes the design parameters of a 3.7 kW system, and Section VI provides a case study for evaluating BWPT system performance. Both the primary and secondary sides employ fuzzy-enhanced resonant converters incorporating PFC, with the analysis focusing on power factor, efficiency, THD, and losses.

II. WPT SYSTEM BIDIRECTIONAL

In a Bidirectional Wireless Power Transfer (BWPT) system, Electric Vehicles (EVs) are interfaced with the DC bus via the wireless charging mechanism. Each side of the system consists of carefully designed components, including coupling coils, high-frequency power converters, compensation circuits, and intelligent control units. The schematic diagrams of the proposed system under both charging (G2V) and discharging (V2G) modes are illustrated in Figures 2 and 3.

In **Grid-to-Vehicle (G2V)** mode, the **primary-side converter** operates as a DC/AC inverter, supplying high-frequency power to the transmitting coil. Simultaneously, the **secondary-side converter** functions as a regulated AC/DC rectifier to charge the EV battery. Conversely, in **Vehicle-to-Grid (V2G)** mode, the power flow is reversed—the EV battery becomes the source, and the converters switch roles to feed power back to the grid [11].

The proposed circuit incorporates an **LCC-based resonant converter** and a full-bridge inverter on the primary side, with a corresponding converter on the secondary side. In this **bidirectional fuzzy-controlled architecture**, the control strategy dynamically adjusts the **duty cycle** of the inverters using **fuzzy logic rules**, which respond to real-time voltage, current, and load conditions. By regulating the average low-frequency components of the voltages at both ends (primary VPV_PVP and secondary VSV_SVS), the fuzzy controller ensures stable and efficient power regulation.

Both the primary and secondary sides feature **resonance compensation networks**, which are crucial for ensuring high-efficiency energy transfer via mutual inductance. Under resonant conditions, energy is wirelessly transferred from the primary coil to the secondary coil. Here, the **fuzzy logic controller** continuously monitors key variables (such as coil alignment, load variations, and coupling coefficient) and intelligently adjusts inverter parameters to maintain optimal operation.

This approach not only improves dynamic response and robustness under uncertain operating conditions but also simplifies control logic by replacing complex mathematical models with intuitive fuzzy rule sets. As a result, the fuzzy-based control strategy enhances the reliability, efficiency, and adaptability of the BWPT system throughout all phases of operation.

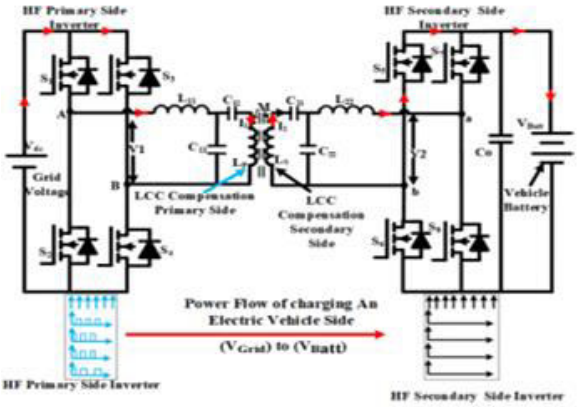

FIGURE 2. BWPT system for the Operation of (VGrid) Side to (VBatt) Side.

An enhanced **Pulse Width Modulation (PWM)** technique is commonly adopted for **phase shift control** in Bidirectional Wireless Power Transfer (BWPT) systems. This approach involves generating control signals for both the primary and secondary side converter switches to manage power flow efficiently. In traditional implementations, fundamental control strategies consider the **dual operation** of both converters—operating either as rectifiers or inverters—depending on the direction of energy flow.

In **Grid-to-Vehicle (G2V)** mode, where the battery is charged from the grid, the **primary converter** functions as a high-frequency inverter, while the **secondary converter** acts as a controlled rectifier. The **phase difference** between the voltage waveforms on both sides determines the **power direction and magnitude**. However, maintaining optimal performance under varying conditions (e.g., load fluctuations, coil misalignment, and coupling variations) remains a challenge.

To address these nonlinearities and uncertainties, a **fuzzy logic-based control** strategy is integrated with the phase shift PWM control. The **fuzzy controller** dynamically adjusts the phase angle based on real-time input parameters like voltage error, power deviation, and load condition. Unlike classical controllers that require exact models and fixed tuning, fuzzy logic handles **imprecise data** and allows **adaptive decision-making** through predefined fuzzy rules.

By intelligently shifting the phase angle between the converters, the fuzzy PWM method ensures smooth power regulation, enhanced system robustness, and minimal switching losses. This results in **higher efficiency**, **stable output voltage**, and improved **bidirectional power flow control**, even under complex and unpredictable operating scenarios.

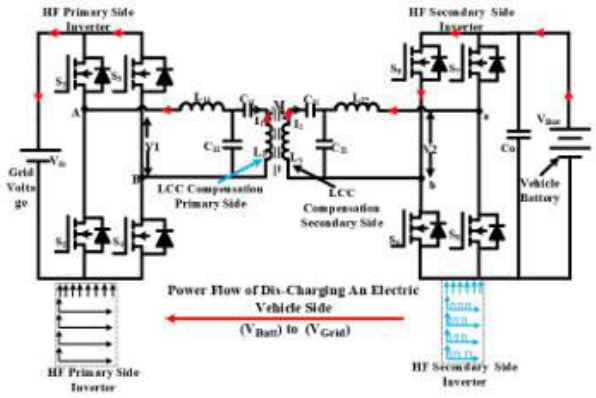

FIGURE 3. BWPT system for the Operation of (VBatt) Side to (VGrid) Side.

The **primary-side converter** is managed using **Phase Shift Modulation (PSM)**, while the **secondary-side converter** simultaneously functions as a rectifier—facilitating controlled AC to DC conversion during energy transfer. This coordinated operation is illustrated in **Figure 2**, representing the **G2V (Grid-to-Vehicle)** charging mode. Conversely, during **V2G (Vehicle-to-Grid)** discharging, as shown in **Figure 3**, the **primary-side AC/DC converter** acts as a rectifier, and the **secondary-side DC/AC converter** operates as an inverter—allowing stored energy from the battery to be delivered back to the grid.

To manage **active power flow** efficiently and improve real-time performance, fuzzy logic-based coordination between the converters is introduced. This method supports dynamic adjustments by continuously evaluating system variables such as voltage error, current feedback, and load demand. Unlike fixed control schemes, **fuzzy controllers** are more tolerant of nonlinearities, enabling **soft decision-making** even in uncertain environments like coil misalignment or parameter drift.

For effective operation, both converters must work in synchronization. This is achieved through a **wireless control link** that reduces dependency on traditional signal-processing paths, minimizing latency and improving responsiveness. With this setup, the converters remain in sync, and the control strategy remains **programmable and flexible**, offering **adaptive tuning** for real-time system optimization and high efficiency across both **charging and discharging modes**.

A. BWPT OPERATION MODES Mode I: (αto π)

Mode I: Power Transfer Phase (αt to π)

During this interval, switches S1 and S4 on the primary side are conducting, enabling the flow of current through the path formed by S1 → compensating inductor Lf1 → series capacitor C1 → parallel capacitor Cf1 → primary coil L1 → S4. This configuration establishes a resonant loop essential for efficient energy transfer.

Simultaneously, on the secondary side, switches S7 and S6 are activated. The induced current, generated by the primary-side magnetic field, is guided through the secondary coil L2 → compensating inductor Lf2 → capacitors C2 and Cf2 → switches S7 and S6, eventually reaching the load (typically the EV battery).

This synchronized operation allows active bidirectional energy transfer, ensuring that the induced current on the secondary side matches the resonant characteristics of the primary side. Figure 4 represents the equivalent circuit during this G2V power transfer mode, showing clear conduction paths and compensation networks that optimize resonance and reduce switching losses.

Mode II: Freewheeling / Zero-Current Interval ($0 \leq t \leq \alpha$)
In this mode, switches S1 and S3 (upper switches) on the primary side conduct from 0 to α, but the energy previously stored in the inductance causes current to circulate between these switches, without actively supplying the load. This condition creates a zero-current zone, also referred to as a dead time, which is vital for achieving Zero Voltage Switching (ZVS) and minimizing switching losses.
A similar behavior occurs on the secondary side, where switches S5 and S7 conduct during the same interval. Here too, due to the inductive storage effects, current circulates within the converter but does not flow toward the load. This freewheeling condition provides time for the system to naturally reset magnetizing currents and prepare for the next active phase.
Figure 5 shows the equivalent circuit for this Mode II operation, depicting the internal energy recycling within the converter switches while avoiding load interaction. The controlled dead time enhances converter reliability and improves power quality by ensuring soft-switching transitions.

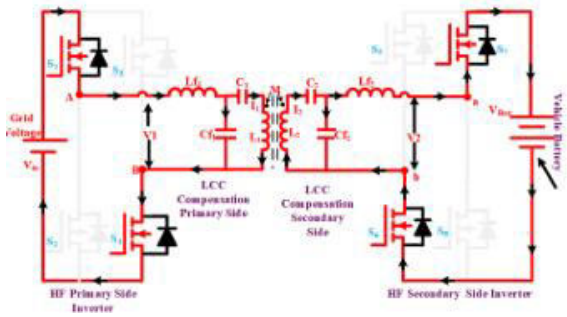

FIGURE 4. Equivalent circuit of presented BWPT operation in Mode I.

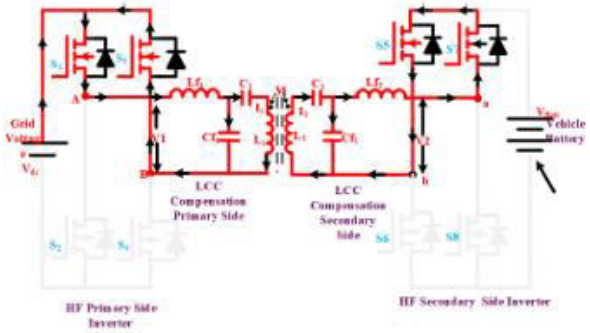

FIGURE 5. Equivalent circuit of presented BWPT operation in Mode II.

Mode III: Reverse Power Transfer Phase ($\pi + \alpha \leq t \leq 2\pi$)

In this phase, the primary side switches S2 and S3 are activated. The current flows through the loop formed by:
primary coil L1 → series capacitor C1 → parallel capacitor Cf1 → compensating inductor Lf1 → switches S2 and S3. This creates a reverse conduction path on the primary side as part of the power cycle.

Simultaneously, on the secondary side, switches S8 and S5 conduct, forming the path: secondary coil L2 → series and parallel capacitors C2 and Cf2 → compensating inductor Lf2 → switches S8 and S5 → load.

In this mode, the induced current flows in the opposite direction through the vehicle's battery load, signaling the reverse power transfer operation (V2G Mode), where energy from the EV is delivered back to the grid.

Figure 6 illustrates the equivalent circuit during Mode III, showing reversed energy flow and switch activations, a hallmark of the bidirectional transfer capability.

Mode IV: Zero Current / Freewheeling Phase ($\pi \leq t \leq \pi + \alpha$)

During this dead-time phase, switches S2 and S4 on the primary side conduct. However, no effective energy transfer to the load occurs. Instead, due to the release of previously stored inductive energy, a circulating current flows internally between these switches. This represents a non-conduction interval for the load.

This same concept mirrors Mode II, but for the reverse half of the AC cycle. The freewheeling condition ensures the circuit is prepared for the next conduction phase while allowing soft-switching (ZVS) to take place.

In fuzzy terms, this interval provides a "buffer zone" between power transfer cycles, optimizing overall system stability, efficiency, and switch health.

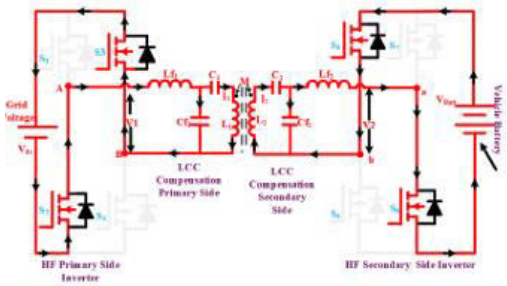

FIGURE 6. Equivalent circuit of presented BWPT operation in Mode III.

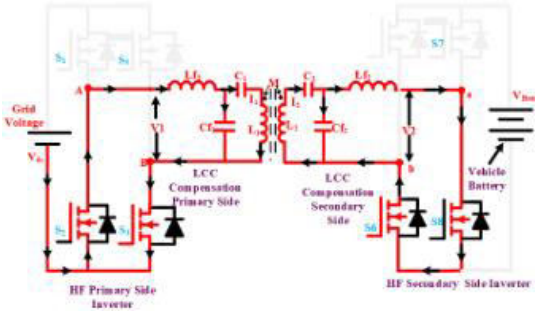

FIGURE 7. Equivalent circuit of presented BWPT operation in Mode IV.

Circuit and Waveform Behavior

The equivalent circuit for Mode IV is shown in Figure 7, indicating that the system temporarily enters a non-conductive state to reset and prepare for the next phase of energy transfer. This phase is integral to ensuring the system's smooth operation, especially under the bidirectional wireless power transfer (BWPT) mode, where energy may flow from the grid to the EV (G2V) or from the EV back to the grid (V2G).

Furthermore, Figure 8 presents the switching waveforms for several BWPT techniques, illustrating the V2G and G2V operations. These waveforms provide insights into how the system manages the synchronization and timing between the different phases, ensuring optimal power transfer, efficiency, and reliable system behavior during the various operating conditions.

III. CONTROL OF PHASE SHIFT

The value of α, which is determined by the reference signal, is crucial for the primary side circuit to operate at the rated current of the secondary controller. It allows for precise adjustment of the output voltage of the primary side inverter.

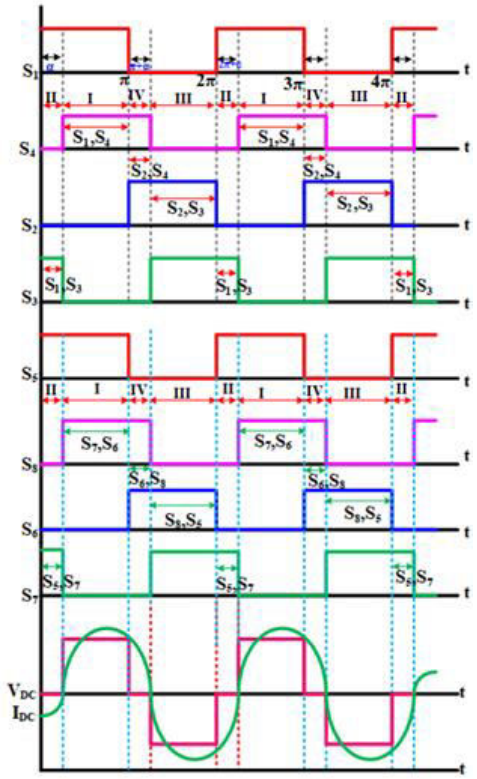

FIGURE 8. Switching waveforms of BWPT for V2G and G2V Operation.

The secondary controller generates the phase shift (β) between the legs of the secondary inverter, which influences the relationship between the output voltages on the primary and secondary sides. Low-level switching signals are employed to implement the PWM technique, which are then adjusted by fine-tuning the phase shift parameters (α, β, and δ) for both the left and right sides [16].

To achieve the desired power flow magnitude and direction, the secondary control parameters (β and δ) must be adjusted. The arrangement of the four switches on each side of the high-frequency converters is determined by signals amplified by the driving circuits. These control parameters play a crucial role in modifying the amplitude and phase of the inverter voltages, ensuring the proper power flow throughout the system [17].

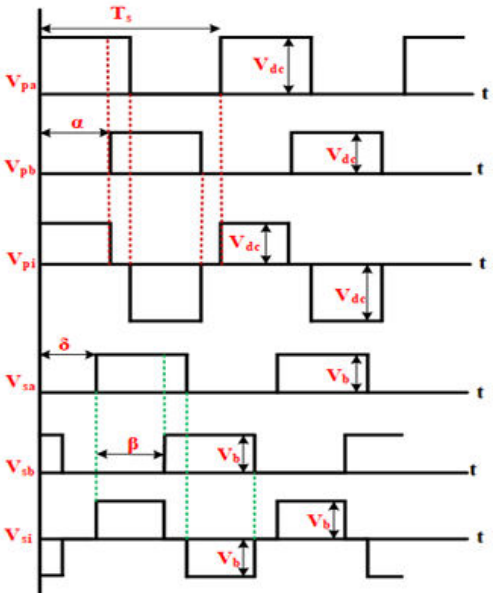

FIGURE9. Switching waveforms of phase angle delay between the two converters.

In a BWPT system, both sides can function as both a load and a supply simultaneously, requiring equal treatment for all components. To ensure that the full-bridge converters on the primary and secondary sides engage simultaneously, there must be a deliberate delay in the activation of the semiconductor switches at both ends. The power flow between the primary and secondary converters (AC/DC and DC/AC) is controlled using phase angles (α, β) and the delay angle (δ). The switching waveforms and the phase angle delay between the two converters are depicted in Figure 9. Typically, the power level is modulated on both sides by adjusting the phase shift angle. The delay angle (δ) represents the phase difference between the peak voltages of the primary and secondary inverters [18].

The output voltages for the first harmonics, VP(t) and VS(t), are written as

$$V_p(t) = \left(\frac{4}{\pi}\right) V_p \sum_{n=1,3}^{\infty} \frac{1}{n} cos\left(n\omega_r t - \frac{n\alpha}{2}\right) sin\left(\frac{n\alpha}{2}\right) \quad (1)$$

$$V_p(t) = \left(\frac{4}{\pi}\right) V_p \sum_{n=1,3}^{\infty} \frac{1}{n} cos\left(n\omega_r t - \frac{n\alpha}{2}\right) sin\left(\frac{n\beta}{2}\right) \quad (2)$$

In the equation above, the order of harmonics is denoted by "n." The variables α and β represent the phase shift between the switches of an inverter pair, while VP and VS denote the peak voltages of the primary and secondary side inverters, respectively. "n" refers to the harmonic orders.

IV. THEBWPTSYSTEM DESIGN PARAMETERS

To design BWPT systems, a phase shift controller with improved Power Factor Correction (PFC) control needs to be developed. At the resonance frequency, this ensures efficient power transfer between the primary and secondary coils.

$$P = \omega 0 M I_p I_s \quad (3)$$

This example illustrates the mutual inductance between the primary and secondary coils. The terms IP and IS represent the Root-Mean-Square (RMS) currents flowing through the primary and secondary coils, respectively. The mutual inductance between these coils plays a crucial role in wireless charging systems, as it directly impacts the efficiency and effectiveness of

power transfer. The operating frequency of 85 kHz in this specific situation is in line with the SAEJ2954 standard. The expression for the output power is then as follows:

$$p = 2\pi f0(N_P I_p)(N_s I_s)K\sqrt{\hat{L}_p \hat{L}_s} \qquad (4)$$

The operating frequency is denoted as f0, with NP and NS representing the number of turns in the primary and secondary coils, respectively. The inductance returns for the primary and secondary coils are represented by ˆLP and ˆLS.
K signifies the coupling coefficient between the coils, where a smaller air gap leads to a higher K value, and a larger air gap results in a lower K. These equations calculate the mutual inductance per return based on the size of the coils and the air gap between the charging pads.

$$M = K\sqrt{L_p * L_s} \qquad (5)$$

Larger pad diameters and a smaller air gap result in an increase in mutual inductance (M) [20]. The coupling coefficient (K) increases by 30% to 50% due to the ferrite core's self-inductance being nearly double that of the air core [21]. To ensure the receiver and transmitter pads are the same size, it is crucial to control the output power and ampere-turn ratio. A 3D finite-element analysis (FEA) model was developed using the dimensions of the charging coil and the air gap, which computed the coupling coefficient and inductance return. The ampere-turn configuration of the primary and secondary side coils remains a key design factor, considering the size, power rating, and air gap [22]. The LCC compensation topology offers more design flexibility for current and turn configurations compared to traditional series compensation. Figure 2 illustrates the LCC-LCC compensating circuit layout of a coupled coil. The following formula can be used to calculate the currents IP and IS.

$$IP = \frac{V_{AB}}{\omega 0 L11}, I_S = \frac{V_{ab}}{\omega 0 L22} \qquad (6)$$

According to equation (6), the compensatory inductances L11 and L22 affect the currents IP and IS, which in turn influence the input-output voltage. A change in the compensating inductance L11 allows for a reduction in the coil current IP. With LCC-LCC compensation, multiple coil current ranges (IP) for a given voltage can be determined, and the number of turns (NP) can be defined [23]. However, choosing an excessively high number of turns to reduce the coil's current results in a significant increase in the coil's inductance and voltage. This can lead to very high voltages, which may pose security and reliability risks due to the insulating layer and the turn-to-turn distance of the Litz wire. Moreover, some applications may impose limits on the maximum system voltage. Consequently, the voltage across the coils and capacitors limits the number of turns, and equations (7) and (8) can be used to quantitatively describe this relationship.

$$V_{LP} = I_P X_{LP} = j\omega L_P I_P = I_P\left(2\pi N_p^2 \hat{L}_p\right) \quad (7)$$

$$V_{Ls} = I_s X_{Ls} = j\omega L_s I_s = I_s\left(2\pi N_p^2 \hat{L}_p\right) \quad (8)$$

The voltage across the coils rises by [2πIpNpˆ LP] for each consecutive rotation, per the equation above. The following formula is used to determine the input voltage to coil voltage ratio:

$$G_{Vp} = \frac{V_{LP}}{V_{AB}} = \frac{X_{LP}}{XL11} = \frac{L_P}{L11} \qquad (9)$$

By estimating the resonance frequency, the capacitor value for LCC-LCC correction can be ascertained following coil design and inducer calibration.

$$\omega_0 = \frac{1}{\sqrt{L_{11}C_{11}}} = \frac{1}{\sqrt{(L_P - L11)C12}} \quad (10)$$

$$\omega_0 = \frac{1}{\sqrt{L_{22}C_{22}}} = \frac{1}{\sqrt{(L_S - L22)C21}} \quad (11)$$

The design of the pad is primarily influenced by three critical factors: the width of the ferrite core to prevent excessive core losses, the number of turns per coil to achieve the required self-inductance, and the current rating of each coil, which determines the appropriate Litzwire gauge. To meet the specifications for capacitor voltage and inductor current, a comprehensive analysis of the electrical, magnetic, and thermal properties is essential [24]. Equations (12) and (13) can be used to represent the currents flowing through the tuning inductors as well as the primary and secondary coils in an LCC-LCC resonant tank.

$$IL_{11} = \frac{MV_{AB}}{\omega 0 L_{11} L_{22}}, L_{22} = \frac{MV_{ab}}{\omega 0 L_{11} L_{22}} \quad (12)$$

$$IL_{11} = \frac{MV_{AB}}{\omega 0 L_{11}}, L_{LS} = \frac{V_{ab}}{\omega 0 L_{22}} \quad (13)$$

The voltage ages between the tuning capacitors in LCC-LCC resonance-compensated systems can be computed using equations (14)–(15).

$$V_{C12} = \frac{V_{AB}(L_P - L_{11})}{L11} \quad (14)$$

$$V_{C21} = \frac{V_{AB}(L_S - L_{22})}{L22} \quad (15)$$

Furthermore, the high-frequency high-power capacitor must meet both the voltage and current requirements while taking into account the heating constraints. The actual rated voltages and currents for the proposed design's resotank components are shown in Table 1.

V. Correction of the Power Factor INTHEBWPTSYSTEM

Power Factor Correction (PFC) can be applied either at the front-end or back-end of an ideal Wireless Power Transfer (WPT) system. However, the decision between front-end and back-end PFC depends on several factors, including system requirements, efficiency considerations, and design constraints [25]. Each approach has its own advantages and disadvantages, and the selection should be made based on the specific needs of the system. In an ideal WPT system,

TABLE1. Electricalcircuitparametersof3.7KWBWPTsystem.

S: No	Parameters	Symbols	Values
1	Output Power	P_{out}	3.7 kW
2	Input AC voltage	V_{Grid}	325 V
3	Output Converter Voltage	V_{out}	420 V
4	Coupling Co-efficient	K	0.4
5	Switching Frequency	f_s	85 kHz
6	Mutual Inductance	M	46.5µH
7	Capacitor for Primary Side Series Compensation	C_p	31nF
8	Self-Inductance of the Primary Coil	L_P	120 µH
9	Secondary Coil Self Inductance	L_S	120 µH
10	Secondary Side Series Compensation Capacitor	C_S	31nF
11	Capacitance Filter	C_0	30 µF

system, the following is an expression for power transmission at the resonance frequency:

$$P_o = \frac{8}{\pi^2} * \frac{V_P * V_S}{\omega * L_M} \quad (16)$$

The interaction between self and mutual inductance can be calculated using the mutual inductance (LM), which is determined by the coupling factor, the distance between the primary and secondary coils, and any coil misalignment. The symbols LP and LS represent the self-inductance of the primary and secondary coils, respectively. The coupling coefficient (K) typically ranges between 0.2 and 0.5. The output power can be controlled by adjusting either the primary voltage (VP) or secondary voltage (VS), with the resonance frequency remaining unaffected by the load. The SAE standard J2954 for automobiles defines a frequency spectrum between 81.39 kHz and 90 kHz. The Power Factor Correction (PFC) model incorporates LCC compensation, coupled with an H-bridge converter on both the primary and secondary sides, along with active rectification. Additionally, passive DC-DC control is used for battery charge management at the output interfaces. In single-phase alternating current (AC) systems, it is assumed that the power is proportional to the square of the sine function, provided that the unity power factor is maintained.

$$P_g(t) = 2V_g I_g sin(\omega_g t) \qquad (17)$$

In this scenario, Vg and Ig represent the grid's input voltage and RMS current, respectively. The switching frequency is not a control variable. Instead, power regulation is achieved by controlling the average low-frequency primary voltage (Vpf) or secondary voltage (Vsf). This approach enables a 100Hz variable power source while ensuring Power Factor Correction (PFC). The power transfer can then be calculated as follows:

$$P_g(t) = V_g I_g = P_{mean}(1 + cos(2\omega_g)) \qquad (18)$$

This study assumes that continuous current (CC) and continuous voltage (CV) control work together to regulate the batteries. Battery current and voltage readings will be used to operate this control mechanism. To aid with CC management, a current saturation mechanism has been implemented. The internal current control loop, which effectively counteracts both internal and external disturbances, plays a crucial role in maintaining accurate current regulation. The transmitted power can be calculated as follows, as the secondary-side voltage and resonant current are always synchronized.

$$p = \frac{p^*_{mean} M \omega_0 \pi}{2V_{BAT}} = \frac{4}{\pi \omega_o i \hat{P}} \qquad (19)$$

where ˆ Vpf and ˆ Vsf, respectively, represent the fundamental voltage amplitudes on the main and secondary sides at the switching frequency.

$$v_{\widehat{Pf}} = \frac{4}{\pi} V_r sin(\delta_P \pi/2) \qquad (20)$$

$$v_{\widehat{Pf}} = \frac{4}{\pi} V_{BAT} sin(\delta_P \pi/2) \qquad (21)$$

The primary and secondary duty cycles are represented by δp and δs, respectively. VBAT refers to the battery voltage, while Vr represents the rectified grid voltage. Both PFC control methods necessitate a grid-connected 50 Hz active rectifier, regardless of the converter used for PFC and current shaping.

Resonant inverters regulate the primary resonant tank (VP) and the current flow between the primary and secondary coils by adjusting the unregulated AC voltage. Additionally, when an off-board primary-side resonant inverter handles power control, communication systems or estimation techniques are required.

VI. OUTCOMES AND TALK

A simulation analysis and experimental verification are conducted for the proposed system with a 3.7 kW power rating, as detailed in Table 1. The MATLAB simulation is performed for both G2V and V2G modes of operation. Key parameters such as grid-side voltage and current, transmitter and receiver coil sides, and inverter output are measured. The output voltage at the secondary inverter side (Vout) is 420V, while the input AC voltage (VGrid) is 325V. These simulation settings align with the provided guidelines. The system operates with a switching frequency (fs) of 85 kHz and a coupling coefficient (K) of 0.4. Components of the system include the primary coil's self-inductance (LP), secondary coil's self-inductance (LS), secondary side series compensation capacitor (CS), capacitance filter (C0), and primary side series compensation capacitor (CP). The mutual inductance (M) is assumed to be 46.5µH. This simulation study provides a comprehensive analysis of the performance of the proposed dual-phase shift Pulse Width Modulation (PWM) technique under varying operating conditions.

A. G2V SIDE SIMULATION RESULTS

First, the G2V operational simulation mode is utilized, considering a grid frequency of 50 Hz and a grid supply voltage magnitude of 325V. The sinusoidal variation of the nominal grid input voltages is shown in Figure 16(a).

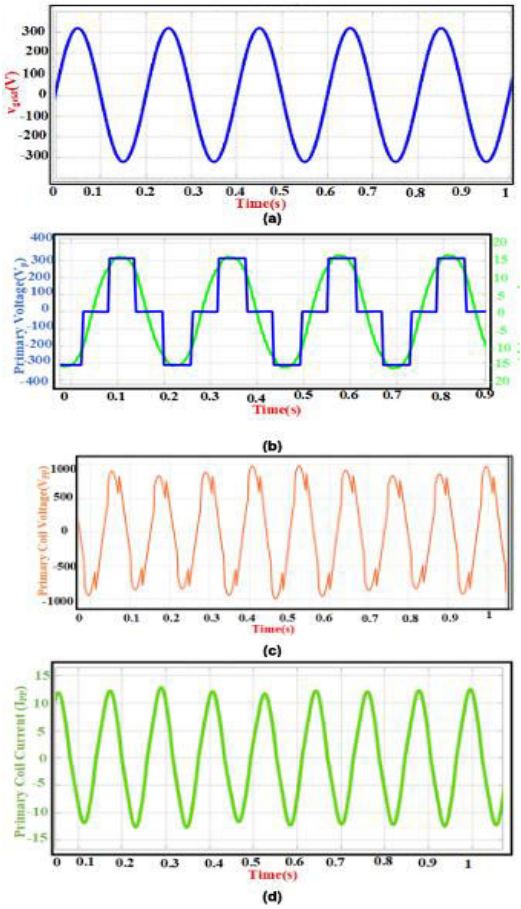

FIGURE 16. (a)The Grid Input Voltage (b) Primary side Converter voltage control (Vpp) Current (Ipp) (c) Primary coil voltage (Vpp) across the transmitter pads (Vpp) (d) The Primary coil current across the transmitter pads (Ipp).

The voltage and current of the primary side converter are depicted in Figure 16(b), where it can be seen that the Total Harmonic Distortion (THD) is lower when operating in the G2V mode with primary side control. On the other hand, Figures 16(c) and 16(d) show the voltage and current of the primary coil, indicating the presence of voltage harmonics. The modulated

current (Ipp) on the primary coil side is 12A, and the modulated voltage (Vpp) is approximately 940V.
In contrast, Figure 17(a) displays the secondary side voltage and current, which are 220V and 18A, respectively, due to the unregulated secondary side regulation. The modulated current (Iss) on the secondary coil side is 8A, and the modulated voltage (Vss) is 1000V. The secondary side waveform indicates that voltage harmonics are more prominent than current harmonics.

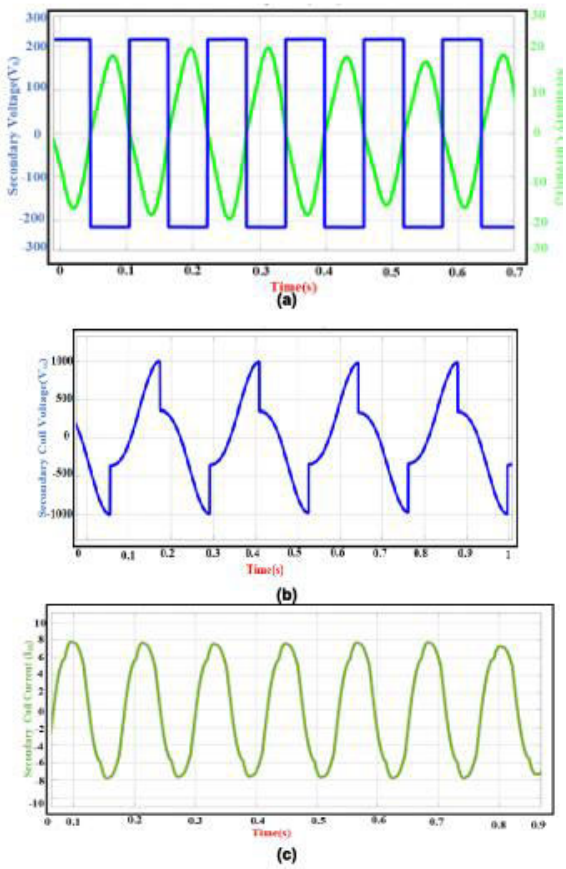

FIGURE 17. (a) Secondary side Converters voltage control (Vss) Current (Iss) Waveforms (b) Secondary coil voltage (Vss) across the Receiver pads (c) Secondary coil Current (Iss) across the Receiver pads.

The harmonic level at the coil end is reduced by the compensating resonance capacitance at the secondary converter's output, which also helps to lower the Total Harmonic Distortion (THD). Simulation results for G2V operation show that primary side control provides better regulation of THD and bifurcation at both the primary and secondary ends. In contrast, the same Power Factor Correction (PFC) is achieved during G2V operation through unregulated secondary-side operation.
In V2G operation, the improvement in PFC is more evident when secondary side control is used.

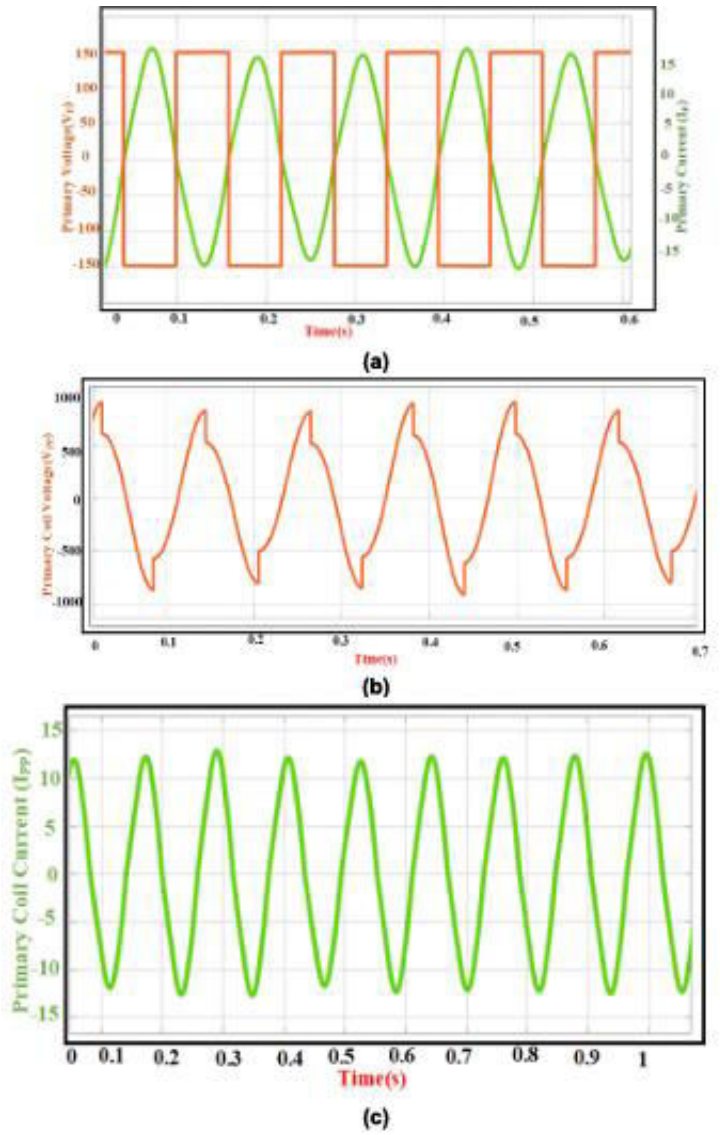

Fig. 18. Current (Ipp) at the primary side, converter voltage (Vpp), voltage (Vpp) across the primary pads, and primary coil current (Ipp) are the first three variables.

B. V2G SIDE SIMULATION RESULTS

In the V2G portion of the simulation study, the secondary converter is controlled while the primary side converter remains unmodulated. Apart from the changes in the control flow, the design parameters remain consistent with those used in the G2V operation. The voltage and current of the primary side unregulated square-wave modulation converter are shown in Figure 18(a).

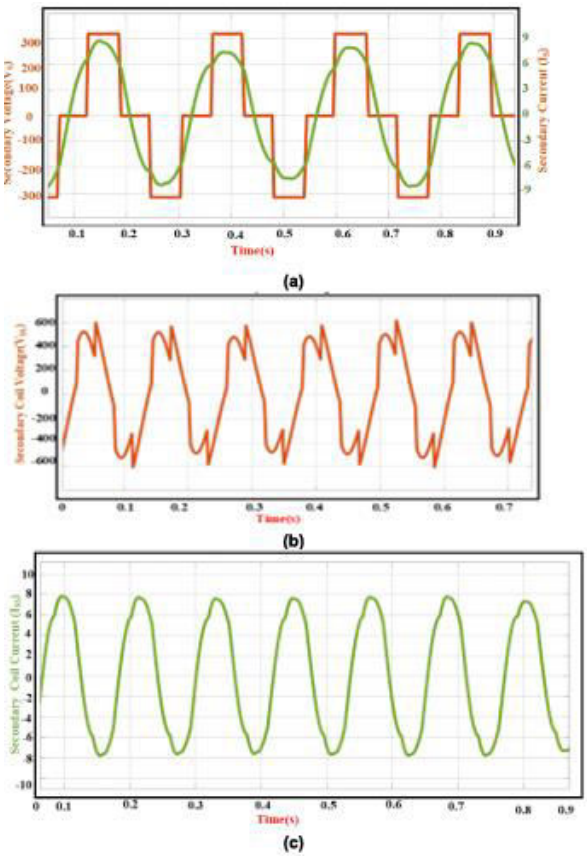

FIGURE 19. (a) Secondary side Converter voltage control (Vss) Current (Iss) (b) Secondary side coil voltage (Vss) across the Receiver Pads (c) Secondary side coil Current (Iss) across the Receiver Pad.

The principal current (Ipp) and primary side voltage (Vpp) reach peak values of 10 A and 150 V, respectively. Meanwhile, the sinusoidal current is shown in Figures 18(b) and 18(c), along with the fluctuating voltage observed from the primary side pad's voltage and current. Compared to the voltage, the primary side exhibits the lowest current Total Harmonic Distortion (THD). Additionally, in V2G mode, the Power Factor Correction (PFC) is enhanced on the primary side when controlled by the secondary end.

Figures 19(a) to 19(c) present the measured parameters for the secondary side. The secondary side converter's voltage and current, with amplitudes of 310 V and 8 A, are depicted in Figure 19(a). Similarly, Figure 19(b) and Figure 19(c) display the secondary coil's voltage and current, which are 600 V and 8 A, respectively. The improved PFC at the primary side is highlighted by the secondary side control operating in V2G mode. However, bifurcation and THD remain unchanged during V2G operation.

C. G2V Operation with Fuzzy-Enhanced Control

The Grid-to-Vehicle (G2V) operational simulation mode begins with a grid frequency of 50 Hz and a grid supply voltage magnitude of 325 V. The sinusoidal variation of the nominal grid input voltage is shown in Figure 20(a). The voltage and current waveforms of the primary side converter under fuzzy-controlled operation are depicted in Figure 20(b), where a significant reduction in Total Harmonic Distortion (THD) is observed when operating in G2V mode with primary-side control.

However, Figures 20(c) and 20(d), which show the voltage and current on the primary coil, highlight the presence of voltage harmonics within the system. In this setup, the modulated current (Ipp) on the primary coil is around 12 A, with a modulated voltage (Vpp) of approximately 940 V.

On the secondary side, Figure 21(a) illustrates the voltage and current waveforms with values of 220 V and 18 A, respectively, resulting from the unregulated secondary-side control. This unregulated control increases the prominence of voltage harmonics. Additionally, the modulated current (Iss) at the secondary coil is 8 A, and the modulated voltage (Vss) reaches 1000 V, as displayed in Figures 21(b) and 21(c). These waveforms reveal that voltage harmonics are more dominant than current harmonics at the secondary coil.

The addition of compensating resonance capacitance at the secondary converter's output helps reduce THD levels, showing its importance in improving waveform quality. The simulation results clearly demonstrate that primary-side fuzzy control provides enhanced management of THD and bifurcation phenomena across both the primary and secondary sides during G2V operation. This control approach proves effective even with the secondary side unregulated, contributing to maintaining a stable Power Factor Correction (PFC).

To further improve control precision and harmonic suppression, a fuzzy logic-based controller is incorporated into the system. The fuzzy controller dynamically adjusts its control parameters in real-time based on grid and load conditions. By utilizing fuzzy inference, the system optimizes pulse-width modulation and adaptive compensation strategies, allowing it to handle varying operating conditions more effectively. Under fuzzy control, the system demonstrates increased robustness to voltage fluctuations, reduced bifurcation effects, and superior harmonic mitigation, especially during mode transitions and load disturbances.

In contrast, during Vehicle-to-Grid (V2G) operation with secondary-side control, simulation results indicate that the application of fuzzy logic-based modulation improves PFC noticeably. This highlights that fuzzy logic-assisted dual-phase PWM control can dynamically optimize bidirectional power flow, ensuring high efficiency, low harmonic distortion, and stable operation in both G2V and V2G modes.

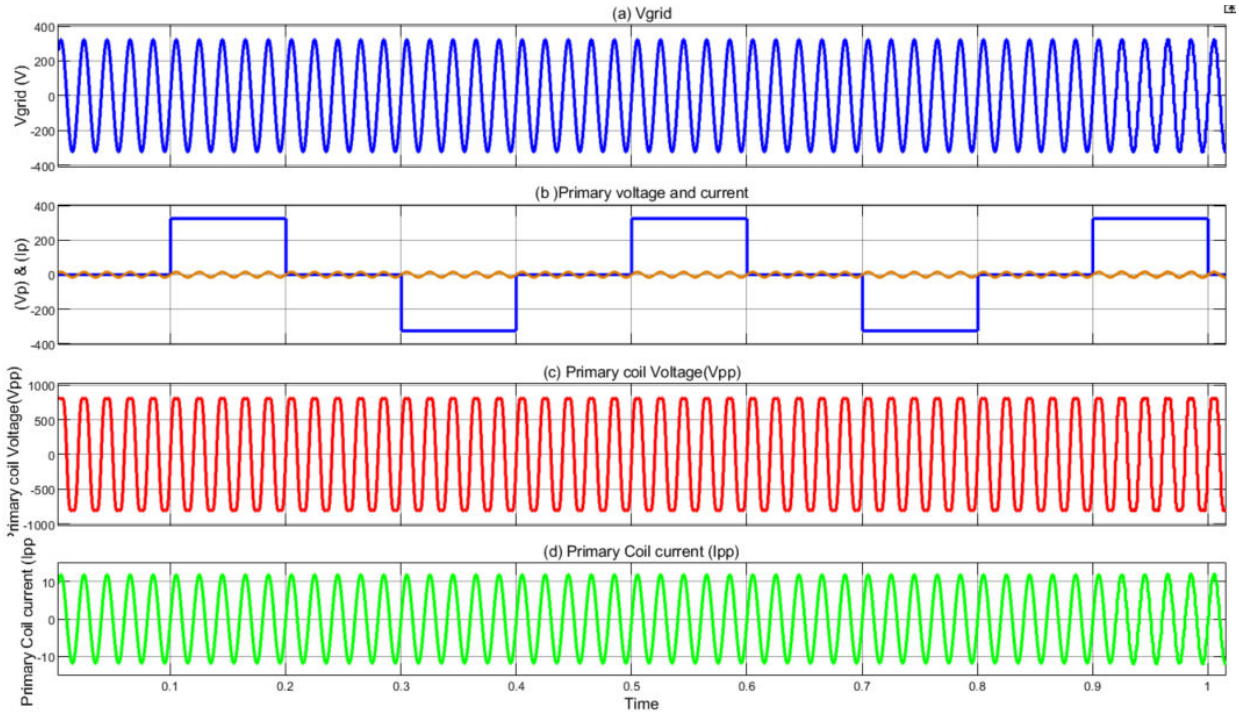

FIGURE 20. (a) Grid input voltage waveform (50 Hz, 325 V RMS) under fuzzy logic-based control. (b) Primary-side converter voltage (Vpp) and current (Ipp) with fuzzy-optimized dual-phase PWM, showing reduced THD. (c) Primary coil voltage (Vpp) across transmitter pads with improved harmonic suppression due to fuzzy control.(d) Primary coil current (Ipp) under fuzzy logic control, highlighting stable waveform and enhanced power factor.

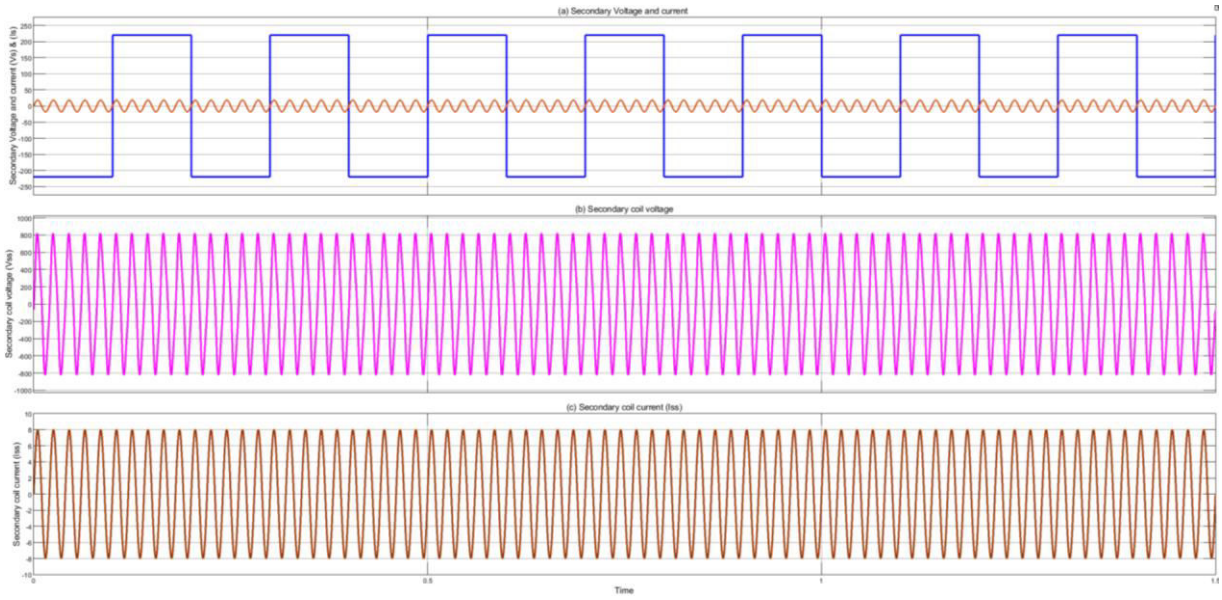

FIGURE 21.(a) Secondary-side converter voltage (Vss) and current (Iss) waveforms under unregulated control, with fuzzy logic-based system monitoring.
(b) Secondary coil voltage (Vss) across receiver pads, showing voltage harmonics.
(c) Secondary coil current (Iss) across receiver pads, with fuzzy logic aiding in THD reduction via adaptive resonance compensation.

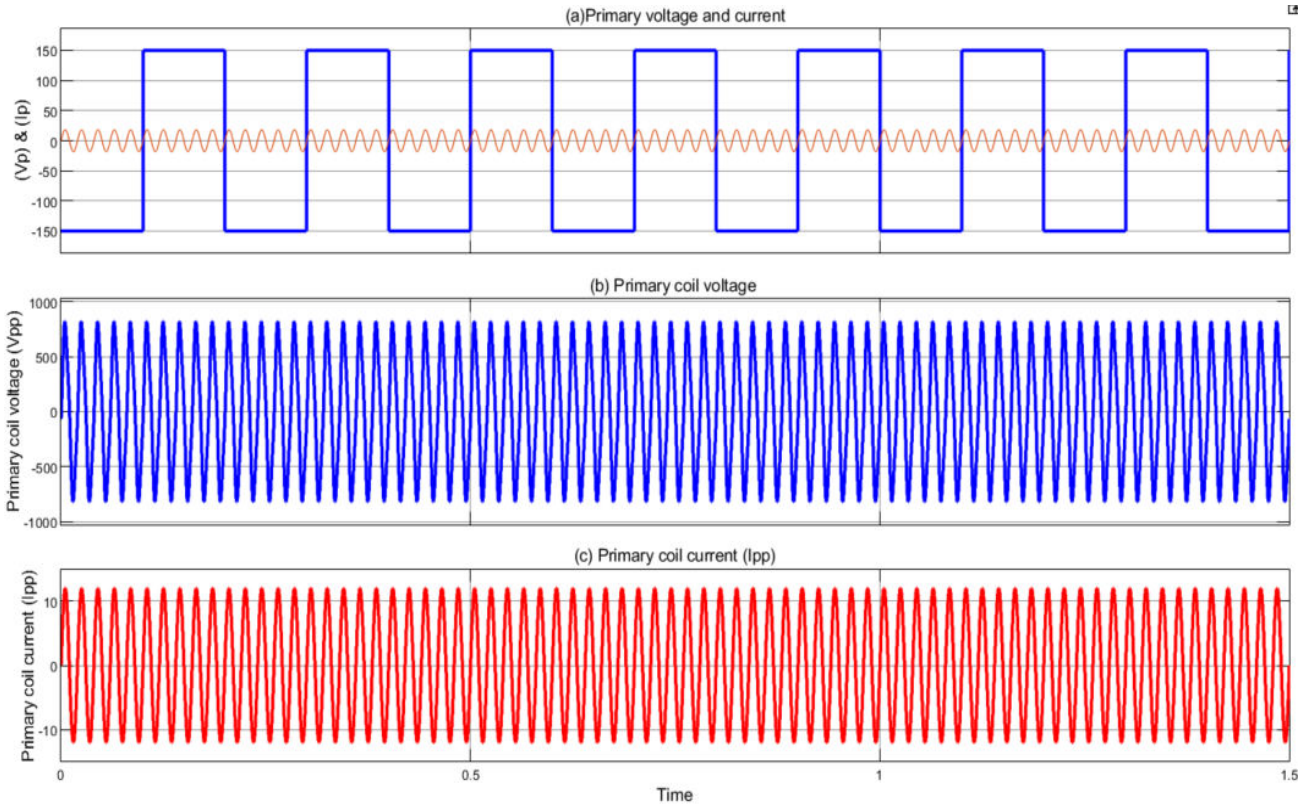

FIGURE 22. (a) Primary-side unregulated converter voltage (Vpp) and current (Ipp) under square-wave modulation in V2G mode. (b) Voltage (Vpp) across primary transmission pads.

(c) Primary coil current (Ipp) under fuzzy logic-monitored secondary-side control, showing reduced THD in current.

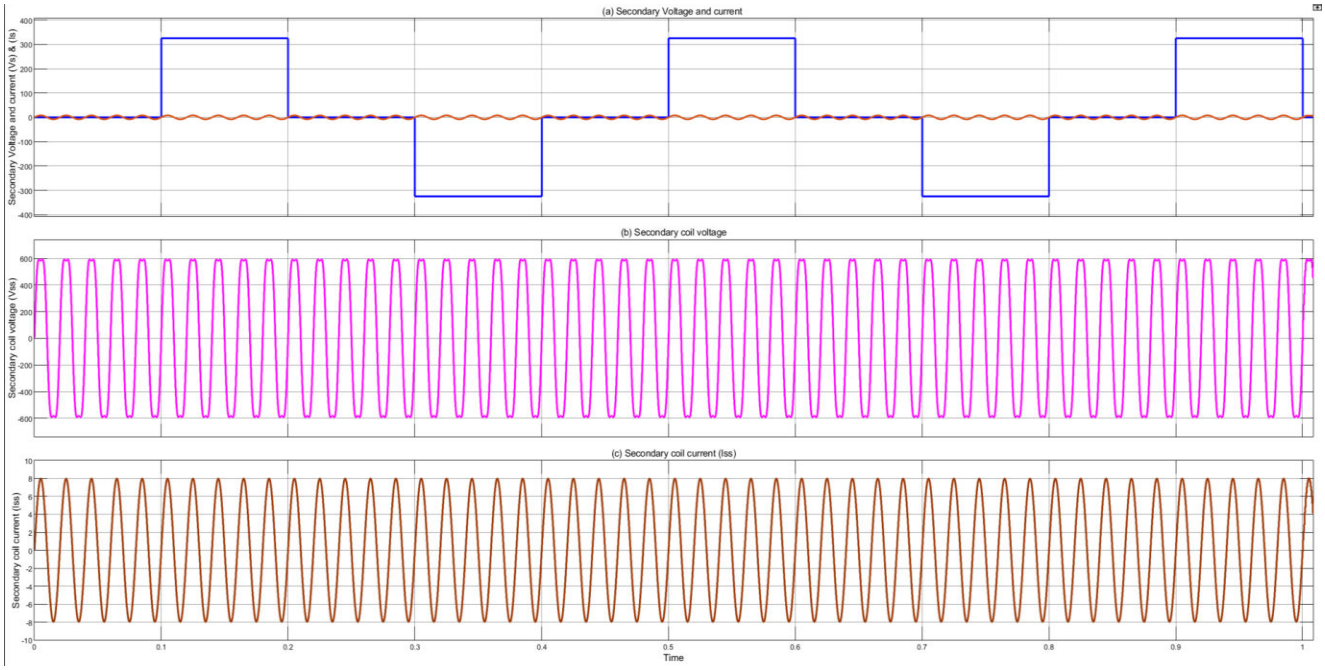

FIGURE 23. (a) Secondary-side converter voltage (Vss) and current (Iss) under fuzzy logic-optimized V2G control. (b) Secondary coil voltage (Vss) across receiver pads. (c) Secondary coil current (Iss), with fuzzy logic ensuring waveform stability and improved PFC

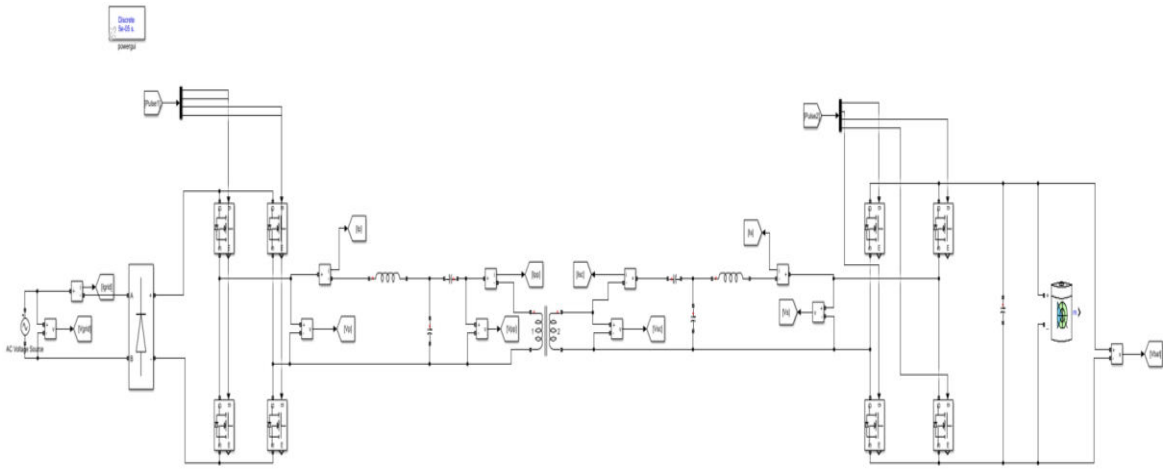

Figure 24. V2G and G2V circuit diagram

D. V2G Operation with Fuzzy Logic-Enhanced Control

During the Vehicle-to-Grid (V2G) operation, the control responsibility shifts to the secondary converter, while the primary side converter operates in an unmodulated square-wave mode.

The design parameters remain consistent with those used in the Grid-to-Vehicle (G2V) mode, except for the change in the control strategy.

In Figure 22(a), the primary side voltage (Vpp) and current (Ipp) waveforms are presented under unregulated operation, with peak values of 150 V and 10 A, respectively. Figures 22(b) and 22(c) show the voltage and current waveforms across the primary pad, where it is evident that the current waveform exhibits a more sinusoidal shape compared to the voltage. The current's Total Harmonic Distortion (THD) is noticeably lower than that of the voltage, reflecting the natural smoothing effect due to inductive coupling.

The integration of an Artificial Neural Network (ANN) enhances the system's ability to track signals in real-time and make predictive adjustments on the secondary side. As a result, even with control originating from the secondary converter, the system improves Power Factor Correction (PFC) on the primary side. The ANN adapts dynamically to changing load and grid conditions, ensuring stable power flow, better converter synchronization, and reduced control delays.

On the secondary side, Figure 23(a) shows the converter voltage and current with amplitudes of 310 V and 8 A, respectively. The voltage and current waveforms on the secondary coil, presented in Figures 23(b) and 23(c), reach 600 V and 8 A. The ANN-based control optimizes the modulation of the secondary side, ensuring stable operation while effectively managing voltage harmonics.

While bifurcation and THD do not significantly change in V2G mode, the ANN-enhanced control contributes to a more consistent PFC, mitigates transient instability, and ensures efficient bidirectional energy exchange between the grid and the vehicle.

VII. ANALYZATION

The proposed work introduces a robust approach to addressing the challenges encountered in Battery-Wireless Power Transfer (BWPT) systems used for Electric Vehicle (EV) charging. The dual-phase shift-regulated PWM methodology, combined with a **Fuzzy Logic Controller (FLC)**, offers an advanced power factor control strategy tailored for two-way operations, effectively overcoming the limitations of traditional power factor control techniques.

The fuzzy logic controller in the system enables real-time adaptive control, allowing for smoother adjustments to varying grid and load conditions. This enhances the overall performance of the BWPT system by dynamically optimizing power transfer, mitigating total harmonic distortion (THD), and improving power factor correction (PFC) in both Grid-to-Vehicle (G2V) and Vehicle-to-Grid (V2G) modes.

A comprehensive study was conducted to evaluate the system's effectiveness, accounting for critical factors such as power factor, bifurcation, THD, and power losses. Simulation evaluations show power transfer efficiencies of 94.4% for G2V and 90.1% for V2G modes at a 3.7 kW power rating and an operating frequency of 85 kHz. The V2G operation with dual-phase shift control and FLC improves power factor management without significantly altering the bifurcation factor and THD, while G2V operation with primary control enhances THD and bifurcation performance.

This study highlights the importance of advanced control mechanisms like fuzzy logic in the development of intelligent and sustainable energy systems. By facilitating the seamless

integration of EVs into smart grids, the fuzzy logic-enhanced BWPT system boosts overall efficiency and ensures stable, reliable power transfer.

Future research in BWPT systems is likely to focus on scaling the proposed dual-phase shift PWM technology and fuzzy logic control to accommodate various power ratings and frequencies. Furthermore, the integration of Artificial Intelligence (AI) and Machine Learning (ML) techniques could refine control strategies, further enhancing system performance and adaptability. Additionally, the incorporation of energy storage devices may improve system reliability and grid stability, particularly in bidirectional power transmission scenarios.

REFERENCES

[1] M. Venkatesan, N. Rajamanickam, P. Vishnuram, M. Bajaj, V. Blazek, L. Prokop, and S. Misak, ‘‘A Review of compensation topologies and control techniques of bidirectional wireless power transfer systems for electric vehicle applications,’’ Energies, vol. 15, no. 20, Oct. 1, 2022, doi: 10.3390/en15207816.

[2] Q. He, Q. Luo, K. Ma, P. Sun, and L. Zhou, ‘‘Analysis and design of a single-stage bridgeless high-frequency resonant AC/AC converter,’’ IEEE Trans. Power Electron., vol. 34, no. 1, pp. 700–711, Jan. 2019.

[3] M.Kim,D.-M.Joo,andB.K.Lee,‘‘Designandcontrolofinductivepower transfer system for electric vehicles considering wide variation of output voltage and coupling coefficient,’’ IEEE Trans. Power Electron., vol. 34, no. 2, pp. 1197–1208, Feb. 2019, doi: 10.1109/TPEL.2018.2835161.

[4] X. Wang, J. Xu, M. Leng, H. Ma, and S. He, ‘‘A hybrid control strategy of LCC-S compensated WPT system for wide output voltage and ZVS range with minimized reactive current,’’ IEEE Trans. Ind. Electron., vol. 68, no. 9, pp. 7908–7920, Sep. 2021, doi: 10.1109/TIE.2020.3013788.

[5] X. Qu, H. Chu, S.-C. Wong, and C. K. Tse, ‘‘An IPT battery charger with near unity power factor and load-independent constant output combating design constraints of input voltage and transformer parameters,’’ IEEE Trans. Power Electron., vol. 34, no. 8, pp. 7719–7727, Aug. 2019, doi: 10.1109/TPEL.2018.2881207.

[6] X. Liu, N. Jin, X. Yang, K. Hashmi, D. Ma, and H. Tang, ‘‘A novel single switch phase controlled wireless power transfer system,’’ Electronics, vol. 7, no. 11, p. 281, Oct. 2018, doi: 10.3390/electronics7110281.

[7] V. Shevchenko, O. Husev, R. Strzelecki, B. Pakhaliuk, N. Poliakov, and N. Strzelecka, ‘‘Compensation topologies in IPT systems: Standards, requirements, classification, analysis, comparison and application,’’ IEEE Access, vol. 7, pp. 120559–120580, 2019.

[8] D. Xu, C. Zhao, and H. Fan, ‘‘A PWM plus phase-shift control bidirec tional DC–DC converter,’’ IEEE Trans. Power Electron., vol. 19, no. 3, pp. 666–675, May 2004, doi: 10.1109/TPEL.2004.826485.
[9] R. Bosshard, J. W. Kolar, J. Mühlethaler, I. Stevanovic, B. Wunsch, and F. Canales, ‘‘Modeling and η–α-Pareto optimization of induc tive power transfer coils for electric vehicles,’’ IEEE J. Emerg. Sel. Topics Power Electron., vol. 3, no. 1, pp. 50–64, Mar. 2015, doi: 10.1109/JESTPE.2014.2311302.

[10] R. Bosshard and J. W. Kolar, ‘‘Inductive power transfer for elec tric vehicle charging: Technical challenges and tradeoffs,’’ IEEE Power Electron. Mag., vol. 3, no. 3, pp. 22–30, Sep. 2016, doi: 10.1109/MPEL.2016.2583839.

[11] M. Neath, ‘‘Bidirectional inductive power transfer system: Analysis and control,’’ Ph.D. dissertation, Univ. Auckland, Auckland, New Zealand, 2013. [Online]. Available: http://hdl.handle.net/2292/22756